The Astrophysical Journal, 1001:182 (7pp), 2026 April 20 https://doi.org/10.3847/1538-4357/ae510a


# Indications of Anisotropy of Cosmic-Ray Elemental Groups Based on KASCADE Data

I. A. Lebedev[1], A. I. Fedosimova[1], Kh. K. Olimov[2], P. M. Krassovitskiy[3], N. O. Yerezhep[3], S. A. Ibraimova[1], and E. A. Bondar[1]
[1] Institute of Physics and Technology, Satbayev University, Almaty, Kazakhstan
[2] Physical-Technical Institute of Uzbekistan Academy of Sciences, Tashkent, Uzbekistan
[3] Institute of Nuclear Physics, Almaty, Kazakhstan
*Received 2025 December 24; revised 2026 March 7; accepted 2026 March 8; published 2026 April 15*

## Abstract

In this work, we study the anisotropy of elemental groups of cosmic rays using data from the KASCADE experiment. The problems of determining primary energy and mass associated with fluctuations in the development of extensive air showers are discussed in detail. To address these issues, a method is used that suppresses the influence of these fluctuations on the estimation of primary energy and mass. The proposed approach is based on the use of lessening fluctuation curves, whose behavior is largely insensitive to shower-to-shower fluctuations during the development of extensive air showers. This allows, firstly, to significantly reduce errors in primary energy estimation and, secondly, to analyze individual showers. The approach also enables simultaneous analysis of showers arriving at substantially different zenith angles $\theta$. To study cosmic-ray anisotropy, we analyzed right ascension versus declination distributions for five elemental groups (p, He, C, Si, and Fe). Analysis of experimental data from the KASCADE collaboration revealed significant differences in the distributions of these groups in equatorial coordinates, which may indicate a directed structure in cosmic-ray fluxes of different elemental composition. The observed features may point to the influence of nearby spiral arms and the Galactic magnetic field structure on the propagation of cosmic rays.

*Unified Astronomy Thesaurus concepts:* Cosmic ray showers (327); High energy astrophysics (739); Particle physics (2088)

## 1. Introduction

Studying the formation and propagation of cosmic rays in the Galaxy requires precise knowledge of their elemental composition and energy spectrum (V. Tatischeff et al. 2021; G. Di Sciascio 2022; N. Arsene 2023).

Numerous studies show that over a wide energy range, the energy spectrum of cosmic rays is described by a power-law dependence $dJ/dE \sim E^{-\gamma}$. Deviations from this dependence are of particular interest. The observed change in the spectral index near energies of $\sim 3 \times 10^{15}$ eV, the so-called knee, has become a key stimulus for the development of theoretical and experimental research (S. P. Swordy et al. 2002; J. R. Horandel 2007).

Recent results of direct experiments lend additional relevance to this problem. This is primarily due to the violation of the power law detected in the proton spectrum at energies of the order of hundreds of GeV. In particular, at an energy of $\sim$13.6 TeV, a change in the spectral index from $\sim$2.60 to $\sim$2.85 was recorded with a statistical significance of $4.7\sigma$ (Q. An et al. 2019). This result may indicate the existence of a new spectral feature of cosmic rays and requires a revision of current concepts of their origin and propagation.

Of additional interest are studies of the inhomogeneity of the spectra of groups of elements at energies above $10^{14}$ eV, measured at ground-based cosmic-ray stations using analysis of extensive air showers (EASs). If irregularities do indeed appear in the proton spectrum at energies of $\sim$13.6 TeV, then similar features may also appear in the spectra of heavier elements at higher energies (A. E. Vladimirov et al. 2012).

Theoretical explanations of the detected inhomogeneity of the cosmic-ray energy spectrum include the contribution of nearby sources (E. Boos et al. 2006; S. Thoudam & J. R. Horandel 2012), the interaction of particles with shock waves (P. L. Biermann et al. 2010), effects due to propagation processes (N. Tomassetti 2012), and the combined effect of multiple acceleration sources (Q. Yuan et al. 2011).

Experimental or reconstruction errors also cannot be ruled out. Significant difficulties are created by fluctuations in the development of cascade processes, which significantly reduce the accuracy of reconstructing the parameters of primary particles. This problem exists both in direct measurements of cosmic rays outside the Earth's atmosphere on spacecraft or high-altitude balloons (E. Dmitrieva et al. 2020; I. Lebedev et al. 2021) and in the analysis of EASs (W. D. Apel et al. 2008) recorded at ground-based cosmic-ray stations. This emphasizes the particular importance of developing methods aimed at reducing the influence of fluctuations in the development of EASs on the results of determining the characteristics of primary cosmic nuclei.

According to the generally accepted view, galactic cosmic rays are formed in supernova explosions (K. Kobayakawa et al. 2002; V. Ptuskin et al. 2013; C. Demidem et al. 2020). Different types of supernovae produce different energy spectra of element groups. Since supernovae are unevenly distributed throughout the Galaxy, anisotropy in the mass composition of cosmic rays can be expected. This anisotropy may be due to both the distribution of sources and the propagation characteristics of charged particles (M. Aglietta et al. 2009; M. Ahlers 2019).

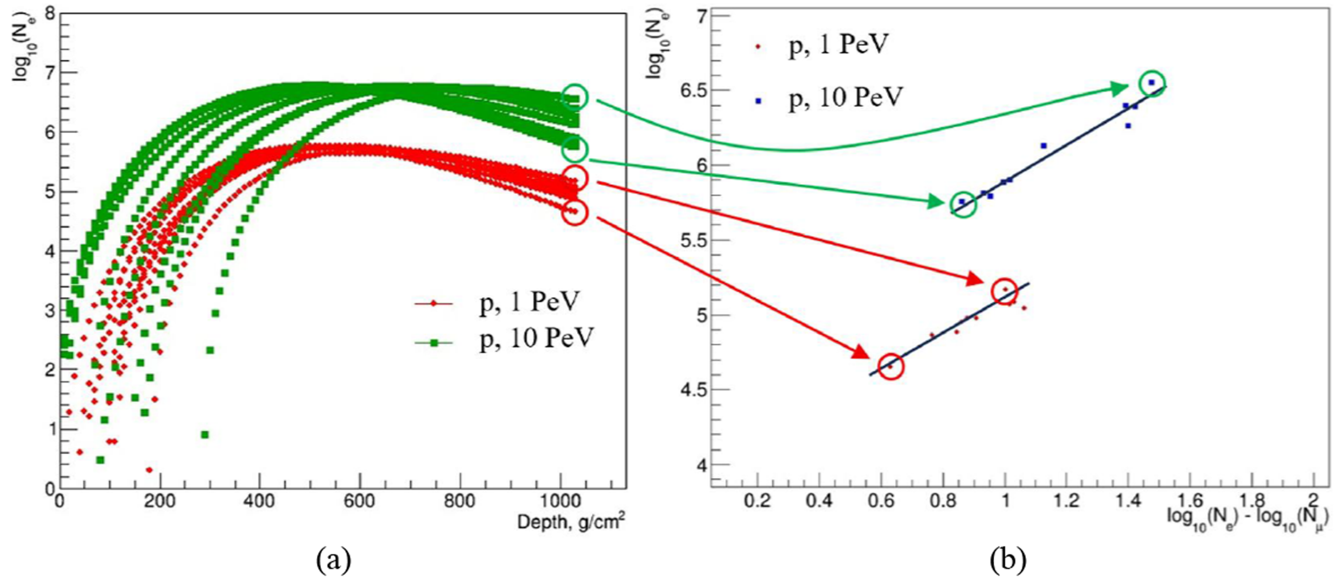


**Figure 1.** (a) Cascade curves for 10 proton-induced air showers at primary energies of 1 PeV (red curves) and 10 PeV (green curves) obtained from CORSIKA simulations and (b) LF curves for the same showers at the observation level of 1023 g $cm^{-2}$.

In this paper, we analyze five elemental groups of cosmic rays (p, He, C, Si, and Fe) in equatorial coordinates using experimental data from the KASCADE collaboration. The primary energy and mass are reconstructed using the lessening fluctuation (LF) curves, whose behavior is largely insensitive to shower-to-shower fluctuations in the development of EASs. This approach enables the simultaneous analysis of cosmic rays arriving at substantially different zenith angles and provides coverage over a wide range of declinations.

## 2. Fluctuations in EAS Development

The information obtained in EAS studies is highly indirect, since the first interaction of a cosmic particle occurs in the upper atmosphere. Consequently, experimenters typically operate not with single events, but with entire ensembles of showers, divided into groups based on the number of electrons at the observation level, which is, on average, proportional to the energy of the primary particle. The analysis involves comparing the average characteristics of a shower group with model calculations, which are usually based on the parameters of an elementary event from accelerator data (R. Engel et al. 2011; K. K. Olimov et al. 2023). Typically, the primary energy $E$ is estimated from the number of secondary electrons $N_e$ at observation level using a relation of the form

$$N_e = \alpha E^{\beta}, \tag{1}$$

where the parameters $\alpha$ and $\beta$ depend on penetration depth and primary mass. This approximation is statistically adequate, but individual $N_e$ values are subject to large fluctuations.

Figure 1(a) shows 10 cascade curves, i.e., log $N_e$ versus atmospheric depth, for proton-induced EASs at primary energies of 1 and 10 PeV. The simulations of EAS development were performed by the authors using the CORSIKA program (D. Heck et al. 1998), version 7.7410, with QGSJETII-04 (S. Ostapchenko 2011) for high-energy ($E_{cm} > 200$ GeV) and FLUKA (A. Fasso et al. 2001) for low-energy ($E_{cm} < 200$ GeV) hadronic interactions.

Analysis of the data presented in Figure 1(a) shows that shower development fluctuates strongly because the depth of the first interaction of a cosmic particle with the nucleus of the Earth's atmosphere varies from event to event. Showers with early first interaction reach their maximum at smaller depths. Such showers can be conventionally termed fast-developing. When the initial interaction occurs in deeper layers, slow-developing showers form, with their maximum shifting to greater atmospheric depths. For the same primary particle energy, slow-developing showers are interpreted using Formula (1) as possessing higher energy, since $N_e$ is greater than the average value. Fast-developing showers, for the same reason, are interpreted as having lower energy. Thus, determining the primary energy solely by the number of electrons at the observation level leads to significant errors in primary energy estimation.

## 3. Lessening Fluctuation Curves

To develop more accurate methods for determining primary energy, it is first necessary to understand the causes influencing the occurrence of large fluctuations in the development of EASs. The problem of fluctuations in the development of EASs is due to the fact that the characteristics of showers recorded at ground level depend not only on the energy and mass of the primary cosmic particle, but also on variations in the parameters of the interaction between the primary cosmic particle and the nucleus of the Earth's atmosphere. These variations govern the initial stages of the cascade process and are intrinsically random (T. N. Kvochkina et al. 2000; A. I. Fedosimova et al. 2024).

First interaction determines the depth at which the cascade begins to develop. The nature of the interaction also has a significant impact: central collisions lead to the formation of a large number of secondary particles and faster cascade development, while peripheral interactions are accompanied by lower multiplicity and slower increase in the number of particles (A. I. Fedosimova et al. 2016; N. Burtebayev et al. 2022). Thus, it is the depth and multiplicity of the first interaction that are the main sources of fluctuations, determining the differences in the initial section of the cascade curve.

The subsequent development of the shower is a chain of successive interactions of secondary particles. Each of these interactions is also subject to random fluctuations. However, due to the large number of interactions, their individual contributions are averaged, and in subsequent stages, the universality of cascade development becomes evident: showers arising from particles of the same energy and mass exhibit, on average, similar characteristics (P. Lipari 2016; A. Fedosimova et al. 2017).

The key difficulty lies in the fact that the depth of the first interaction and its associated parameters are highly unreliable due to strong stochastic fluctuations.

To reduce the influence of these fluctuations, instead of the penetration depth, it is necessary to use a parameter that characterizes the development of the cascade as a whole and is less dependent on the initial random factors.

In I. Lebedev & E. G. Boos (2003), the shower age parameter $s$ was introduced instead of the penetration depth. From a physical point of view, the age parameter represents the evolutionary stage of the cascade, rather than its geometrical development in the atmosphere. While the depth of the shower maximum fluctuates strongly from event to event due to stochasticity of the first interactions, the maximum of the cascade in age coordinates is a universal feature of cascade dynamics and is always located at $s = 1$. This reflects the fact that the condition of maximum particle multiplication is determined by cascade physics itself and not by the particular realization of the initial interaction. As a result, the representation $\log N_e$ ($s$) naturally suppresses shower-to-shower fluctuations and provides a physically stable description of shower development.

A similar physical principle underlies the approach proposed by E. Dmitrieva et al. (2020) and S. A. Ibraimova et al. (2025), where the parameter $dN = \log N_e(Z_1) - \log N_e(Z_2)$ is used instead of the penetration depth. This quantity characterizes the local longitudinal development of the cascade between two observation levels $Z_1$ and $Z_2$ separated by an absorber. In this representation, the cascade maximum corresponds to a universal condition $dN = 0$, reflecting the balance between particle production and attenuation, and is therefore independent of shower-to-shower fluctuations in the first interaction.

In the present work, we use LF curves, defined as the dependence of $\log N_e$ on

$$dN_{em} = \log N_e - \log N_\mu, \quad (2)$$

where $N_e$ and $N_\mu$ are the numbers of electrons and muons, respectively.

This method was previously applied in our joint analysis with the KASCADE collaboration (W. D. Apel et al. 2008).

Figure 1(b) shows the corresponding LF curves for the same proton showers as in Figure 1(a) at the observation level of 1023 g cm$^{-2}$. An analysis of Figure 1(b) indicates that the simulated events are distributed along well-defined LF curves. These curves reflect the general patterns of EAS development, largely independent of random fluctuations in the depth and multiplicity of the first interaction.

Quantitatively, the LF method strongly suppresses shower-to-shower fluctuations. For the 10 PeV proton showers shown in Figure 1(a), the spread in $\log N_e$ between the maximum and minimum is 0.768. In the LF representation (Figure 1(b)), deviations from the LF curve are roughly 10 times smaller, demonstrating that using $dN_{em}$ instead of the penetration depth reduces the effect of early-stage fluctuations by 1 order of magnitude.

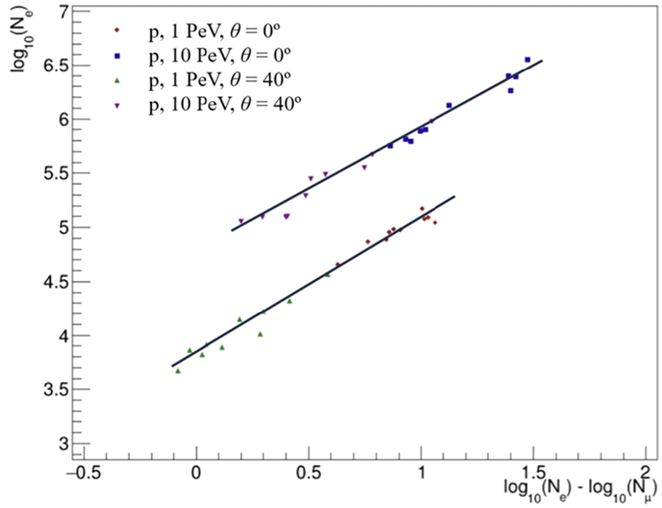


**Figure 2.** LF curves for simulated proton extensive air showers with energies of 1 and 10 PeV and zenith angles of 0° and 40°.

From a physical perspective, both components originate from the same hadronic cascade: neutral pions decay into photons and generate the electromagnetic component, while charged pions and kaons decay into muons and neutrinos, forming the muonic component. Because both components are produced in the same hadronic interactions, their fluctuations are strongly correlated. Consequently, the ratio between the electromagnetic and muonic components encodes the global state of cascade development, rather than the stochastic properties of the first interaction. As a result, the representation $\log N_e$ ($dN_{em}$) is practically insensitive to early-stage cascade fluctuations, and the measured values of $\log N_e$ remain tightly clustered around the mean LF curve. This demonstrates that LF curves provide a physically motivated and robust description of shower evolution, in which the dominant source of fluctuations related to the depth and multiplicity of the first interaction is strongly suppressed by the construction of LF curves.

It is particularly important to note that the LF curves corresponding to different primary particle energies are spatially separated. This means that showers with energies of, for example, 1 and 10 PeV form families of points located at a noticeable distance from each other. This separation allows for direct comparison of experimental data with calculated models and significantly improves the accuracy of primary particle energy reconstruction.

Another useful property of LF curves is the ability to simultaneously analyze EASs arriving at significantly different zenith angles $\theta$.

Figure 2 shows LFmcurves for proton showers with $\theta = 0°$ and $\theta = 40°$.

Analysis of the data presented in Figure 2 shows that EASs initiated by primary particles of the same energy, even at significantly different zenith angles, are located along the same LF curves.

Reconstruction of the primary energy using Equation (1) depends on the zenith angle due to atmospheric attenuation effects on $N_e$. The value of $N_\mu$ at the observation level also exhibits a strong dependence on $\theta$. Therefore, the simultaneous analysis of EASs arriving at substantially different zenith angles is particularly challenging, since it requires accurate corrections for the attenuation effects in both $N_e$ and $N_\mu$. As the zenith angle $\theta$ increases, the shower's path length in the atmosphere increases, resulting in the effective thickness of the atmospheric layer at $\theta = 40^\circ$ being approximately 1.3 times greater than in the vertical direction. This shifts the position of the cascade maximum toward greater atmospheric depths, altering the shape of the cascade curve and, consequently, requiring complex corrections when reconstructing shower parameters.

In contrast, the variable $dN_{em}$ is physically insensitive to the geometrical propagation effects in the atmosphere. Both the electromagnetic and muonic components originate coherently from the same hadronic cascade and evolve in a strongly correlated manner. Although $N_e$ and $N_\mu$ individually depend on atmospheric depth, their correlated evolution leads to an atmospheric-depth–independent parameterization of shower development in $dN_{em}$.

Thus, using the $dN_{em}$ parameter as a universal variable not only smooths out individual fluctuations and ensures energy separation of events, but also enables the correct joint analysis of showers arriving at significantly different zenith angles. This allows us to move from the analysis of highly fluctuating cascade curves to more stable and informative relationships. From a practical standpoint, this means that uncertainties associated with the random nature of primary interactions and variations in the initial stage of cascade development have a significantly smaller impact on the reconstruction results. This ultimately leads to a more reliable determination of the energy of primary cosmic particles and paves the way for refining their mass composition.

## 4. Approach to Primary Mass Estimation

The number of muons in EASs is often used to determine the mass of the primary cosmic particle. This method is based on the fact that light and heavy nuclei form different muon components when interacting with the Earth's atmosphere. All other things being equal, the higher the mass number $A$ of the primary nucleus, the more muons are produced in the shower. This is because heavy nuclei begin to interact with the atmosphere at higher altitudes and decay into a greater number of nucleons. Each subsequent interaction produces cascades of particles, including pions, which then decay into muons. A significant drawback of this method is its high sensitivity to fluctuations in cascade development: showers initiated by protons of the same energy can contain significantly different numbers of muons at the observation level.

To address the problem of fluctuations, following the approach described above, we introduce $dN_{em}$ as an additional variable which allows us to effectively suppress the influence of fluctuations. The log $N_\mu$ versus $dN_{em}$ dependencies are hereafter referred to as LF curves for mass reconstruction (or LFM curves).

Figure 3 shows LFM curves for proton and iron showers at 1 and 10 PeV and zenith angles of 0° and 40° at an observation level of 1023 g cm$^{-2}$. In this representation, proton and iron points separate not only by $N_\mu$ but also by $dN_{em}$, which increases the discrimination power.

For example, a proton shower with log $N_\mu = 4.17$ and $dN_{em} = 0.996$ is well separated from an iron shower with log $N_\mu = 4.17$ and $dN_{em} = 0.402$, although they cannot be distinguished using $N_\mu$ alone, since it is the same for both showers.

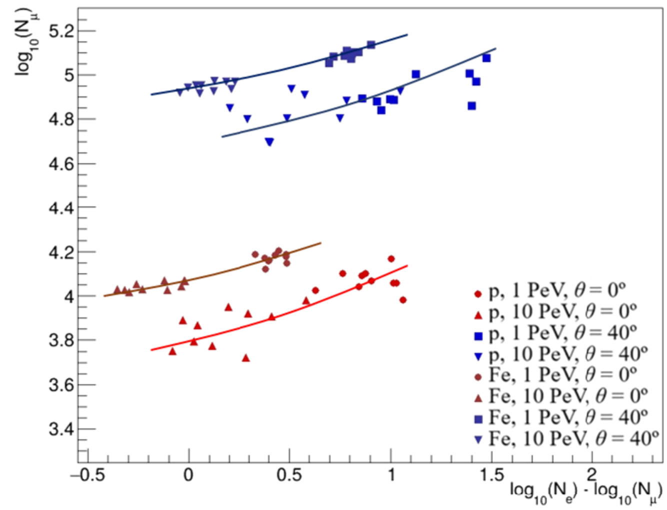


**Figure 3.** LFM curves for proton and iron showers with energies 1 and 10 PeV and zenith angles of 0° and 40° at an observation level of 1023 g cm$^{-2}$.

## 5. Analysis Procedure

For the analysis, simulation datasets from the KASCADE Cosmic Ray Data Center (A. Haungs et al. 2018) were used, based on the hadronic interaction models QGSJETII-04 and FLUKA (version 2012.2.14_32).

The dataset contains approximately one million EASs in the energy range from $10^{14}$ to $10^{18}$ eV for each of the five primary species (p, He, C, Si, and Fe). The energy distribution follows a power-law spectrum with a spectral index of −2. The zenith angles are distributed in the range [0°–42°].

LF curves were built for fixed energies by fitting simulation data with third-order polynomials. Then the polynomial coefficients were parametrized as functions of energy to obtain an LF function for primary energy calculation:

$$\log N_e(dN_{em},\ E) = a_0(E) + a_1(E)dN_{em} + a_2(E)dN_{em}^2 + a_3(E)dN_{em}^3. \quad (3)$$

Primary energy was determined by varying $E$ and minimizing the difference between the function log $N_e$ ($dN_{em}$, $E$) and the measured log $N_e$ given the measured $dN_{em}$.

Similarly, a function for muon number for proton showers was obtained:

$$\log N_\mu{}^{\mathrm{p}}(dN_{em},\ E) = b_0(E) + b_1(E)dN_{em} + b_2(E)dN_{em}{}^2 + b_3(E)dN_{em}{}^3. \quad (4)$$

The primary mass $A$ was determined by the formula

$$\log A = c_0(E) + c_1(E)(\log N_\mu{}^{\mathrm{A}} - \log N_\mu{}^{\mathrm{p}}), \quad (5)$$

where $c_0(E)$ and $c_1(E)$ are parameters obtained from simulations.

The numerical values of these coefficients for primary energies of 1 and 10 PeV are presented in Table 1.

Figure 4 shows the obtained accuracies of the primary mass and energy reconstruction, whose uncertainty estimates are comparable to the results of our previous study (W. D. Apel et al. 2008).

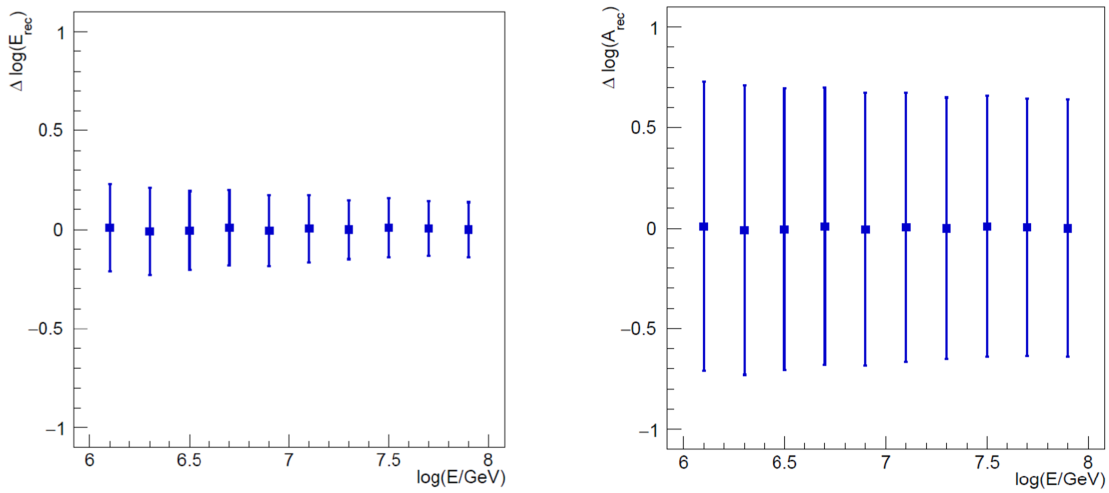


**Figure 4.** Left: accuracy in energy reconstruction. Right: accuracy in mean mass reconstruction. The full Monte Carlo sample of five primary mass groups with equal abundances was used.

**Table 1**
Coefficients for Equations (3)–(5) Used for Primary Energies of 1 and 10 PeV

| E | 1 PeV | 10 PeV |
|---|---|---|
| $a_0$ | 3.856 ± 0.009 | 4.803 ± 0.017 |
| $a_1$ | 1.180 ± 0.050 | 1.030 ± 0.069 |
| $a_2$ | 0.212 ± 0.094 | 0.357 ± 0.084 |
| $a_3$ | −0.181 ± 0.049 | −0.193 ± 0.032 |
| $b_0$ | 3.884 ± 0.001 | 4.744 ± 0.003 |
| $b_1$ | 0.258 ± 0.004 | 0.207 ± 0.028 |
| $b_2$ | 0.043 ± 0.011 | 0.031 ± 0.093 |
| $b_3$ | −0.036 ± 0.036 | −0.029 ± 0.086 |
| $c_0$ | 0.008 ± 0.013 | −0.004 ± 0.006 |
| $c_1$ | 8.304 ± 0.102 | 8.750 ± 0.055 |

Using this approach, we investigated anisotropy of elemental groups based on experimental KASCADE data.

## 6. Anisotropy of Cosmic-Ray Elemental Groups

Anisotropy reflects the directional unevenness of particle fluxes of varying compositions and serves as a sensitive indicator of the spatial distribution of sources and diffusion characteristics in the Galaxy. Since the distribution of cosmic-ray sources is closely related to the structure of the spiral arms, it is advisable to analyze directional anisotropy in the equatorial coordinate system. This approach allows for a direct correlation of observed directions with astronomical objects and galactic structures.

This study analyzes the R.A. ($\alpha$) versus decl. ($\delta$) distributions, which allows for the identification of possible anisotropic deviations and their comparison for different elemental groups. The ability to simultaneously analyze EASs arriving at significantly different zenith angles $\theta$ opens up prospects for studying cosmic-ray anisotropy over a wide range of $\delta$. Using reconstructed energy and mass parameters of primary particles allows for the separation of events by composition and clarification of the relationship between the chemical composition of cosmic rays and their galactic sources.

Experimental data from the KASCADE Cosmic Ray Data Center were used for the analysis (A. Haungs et al. 2018). For the analysis, quality cuts were applied, as in T. Antoni et al. (2005) and W. D. Apel et al. (2008). Only measurement runs with all clusters active are considered. To avoid threshold effects, only showers with shower sizes $\log N_e > 4.8$ are included. In total, the used sample sums up to 993 days of measuring time. The total number of events amounts to $7.6{\cdot}10^5$.

For each EAS, the primary energy was determined using Formula (3), and the primary particle mass was estimated using Formulas (4) and (5).

To investigate the anisotropy of cosmic rays as a function of their elemental composition, all events were classified into five representative mass groups: p, He, C, Si, and Fe. This grouping follows the standard convention adopted in KASCADE analyses (W. D. Apel et al. 2013).

The classification was performed in terms of the logarithm of the atomic mass number, $\ln A$, which provides an approximately linear dependence of shower observables on the primary mass. The adopted boundaries correspond to the following ranges: protons $\ln A < 0.7$, helium $0.7 \leqslant \ln A < 2.0$, C $2.0 \leqslant \ln A < 3.0$, Si $3.0 \leqslant \ln A < 3.7$, and iron $\ln A \geqslant 3.7$.

The boundary between the proton and helium groups ($\ln A = 0.7$) represents the mid-point between the mean logarithmic masses of hydrogen ($\ln A = 0$) and helium ($\ln A = 1.39$).

Figure 5 presents the distributions of EAS events over R.A. and decl. for the five elemental groups. The plots show the fraction of showers of each elemental group normalized to the total number of events in a given cell of the sky. The choice of plotting decl. along the $x$-axis was motivated by the intention to facilitate the comparison of relative variations between decl. bands and to highlight regions with different fractional contributions of elemental groups.

The analysis of Figure 5(a) shows that in the central region with declinations $\delta$ from 30° to 60°, the proton fraction is significantly smaller than in regions with $\delta < 30°$ and $\delta > 60°$. The helium, C, and Si groups show opposite trends with enhanced content in the central band (Figures 5(b)–(d)), while the heaviest elements (Fe) show the largest share at declinations below 30° (Figure 5(e)).

Differences in the distribution of elemental groups are likely related to the anisotropy of galactic cosmic rays, caused by the nonuniform distribution of their sources and the peculiarities of particle transport in the galactic magnetic field.

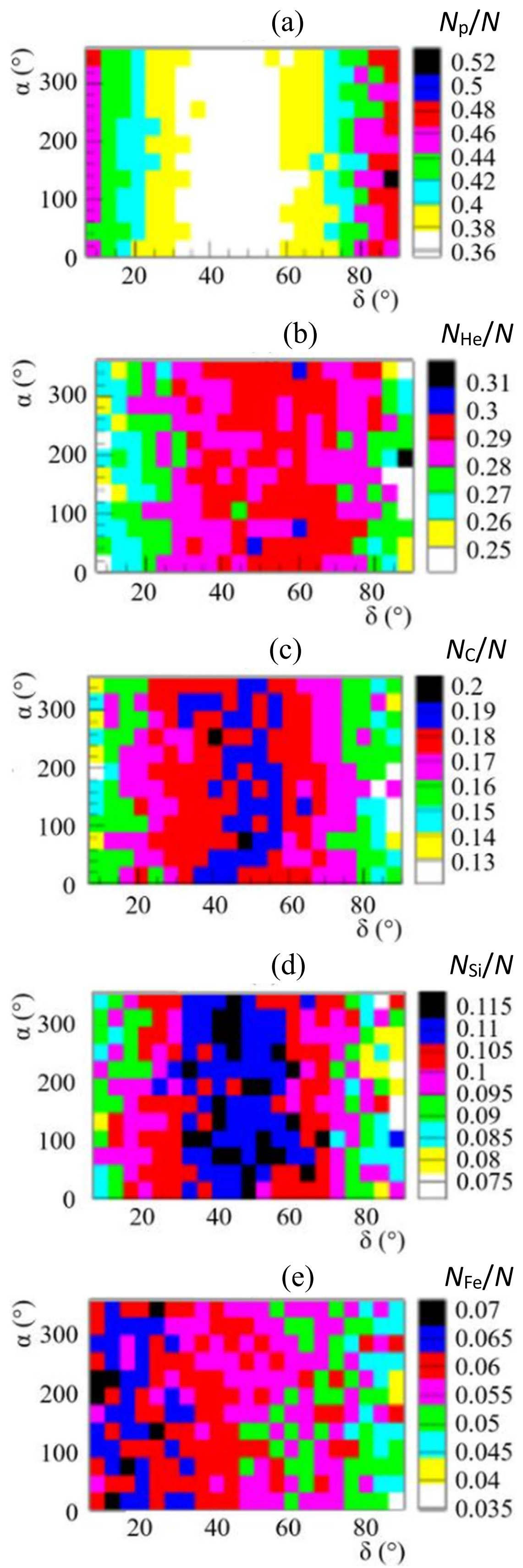


**Figure 5.** Distributions over R.A. ($\alpha$) and decl. ($\delta$) of the fractional contribution of each elemental group, normalized to the total number of events in each sky cell: (a) p; (b) He; (c) C; (d) Si; and (e) Fe.

The regular magnetic field of the Milky Way is known to have a spiral structure similar to the structure of the galactic arms. This field significantly influences the trajectories of charged particles, causing their diffusion and deflection depending on their charge and energy (P. G. Tinyakov & I. I. Tkachev 2002; G. Giacinti et al. 2018). Heavier nuclei, possessing a higher charge, interact more strongly with the magnetic field and exhibit a more pronounced localization in directions coinciding with areas of cosmic-ray source concentration (for example, along spiral arms).

Conversely, protons, possessing a lower charge and, consequently, a longer mean free path, are capable of propagating over greater distances, forming a relatively uniform distribution and an increased fraction in regions distant from the main sources.

It should be noted that the R.A. and decl. distributions presented in this work reflect the relative fractions of different elemental groups and are intended exclusively for qualitative (not quantitative) illustration of possible directional trends associated with the mass composition of cosmic rays.

The KASCADE experiment provides long-term stable operation, and due to the Earth's rotation, the exposure in R. A. is approximately uniform. The LF method allows the inclusion of air showers over a wide range of zenith angles, thereby extending the accessible decl. range. At the same time, the number of registered events depends on the arrival direction because of a combination of effects, including geometrical suppression (reduced effective detection area at large zenith angles), atmospheric attenuation (the increased atmospheric path length reduces the number of secondary particles reaching the detectors), and geomagnetic effects, including the east–west effect, which leads to a suppression of low-energy particles arriving from the eastern direction relative to the western one.

Consequently, the analysis does not focus on the absolute number of particles of each elemental group arriving from a given direction on the celestial sphere, but rather on the percentage fraction of a given elemental group within the total number of particles registered from that direction.

In addition, systematic uncertainties can affect both the reconstruction of primary energy and mass composition. Possible sources include uncertainties in the energy reconstruction due to shower-to-shower fluctuations and hadronic interaction models, misclassification between elemental groups in mass reconstruction, and selection biases introduced by quality cuts. These systematic effects primarily influence the absolute values of energy and mass, but are expected to have a smaller impact on the qualitative trends observed in the relative fractions of elemental groups.

We therefore emphasize that the observed features in the distributions of elemental groups in R.A. and decl. should be interpreted as indications of possible anisotropy in the elemental composition, rather than as a quantitative measurement of cosmic-ray anisotropy.

## 7. Conclusions

In this paper, the anisotropy of elementary groups of cosmic rays is studied using data from the KASCADE experiment. It is noted that the results of the analysis can significantly depend on the accuracy of determining the primary energy and mass.

Therefore, the problems associated with determining these parameters are examined in detail. The primary focus is on fluctuations in the development of EASs. The key difficulty is that cascade curves and their associated parameters (log $N_e$ at the observation level) are unreliable due to strong random variations in the depth and multiplicity of the first interaction. Therefore, determining the primary energy solely from the number of electrons at the observation level leads to significant errors.

For calculations, this paper uses a technique that suppresses the influence of fluctuations in the development of EASs on the estimate of the primary particle energy. The proposed approach is based on the use of certain lessening fluctuation curves, log $N_e$ versus $dN_{em}$, whose behavior is independent of fluctuations in the development of EASs. Using the $dN_{em}$ parameter as an additional variable significantly suppresses the influence of fluctuations, which are much more pronounced when using only log $N_e$.

Using the $dN_{em}$ parameter as the first interaction independent variable not only smooths out individual fluctuations but also ensures energy separability of events. This enables a transition from the analysis of highly fluctuating cascade curves to more stable and informative dependences. This allows, first, to significantly reduce errors in determining the primary energy and, second, to analyze individual showers. Ultimately, the prerequisites for refining the mass composition of cosmic rays are created.

The number of muons in EASs is often used to determine the mass of the primary cosmic particle. This article shows that accuracy can be significantly improved by using the dependence of log $N_\mu$ versus $dN_{em}$.

Another useful property of LF curves is the ability to correctly jointly analyze EASs arriving at significantly different zenith angles $\theta$. To study cosmic-ray anisotropy, an analysis of the R.A.–decl. coordinate plane distributions for five elemental groups (p, He, C, Si, and Fe) was performed using experimental data from the KASCADE collaboration. Significant differences in the distribution of these groups in equatorial coordinates were identified, which may indicate the presence of a directional structure in cosmic-ray fluxes of different elemental compositions. These features in the distribution of elemental groups may indicate the influence of the nearby spiral arms of the Galaxy and the structure of its magnetic field on the propagation of cosmic rays.

## Acknowledgments

This work was supported by the Ministry of Science and Higher Education of the Republic of Kazakhstan (grant No. AP23488106).

## ORCID iDs

I. A. Lebedev https://orcid.org/0000-0002-7562-9925
A. I. Fedosimova https://orcid.org/0000-0001-9607-6074
Kh. K. Olimov https://orcid.org/0000-0002-1879-8458
P. M. Krassovitskiy https://orcid.org/0000-0001-8145-7974
N. O. Yerezhep https://orcid.org/0000-0002-7457-2189
S. A. Ibraimova https://orcid.org/0000-0002-6652-9252
E. A. Bondar https://orcid.org/0000-0001-6745-5462

## References

Aglietta, M., Alekseenko, V. V., Alessandro, B., et al. 2009, ApJ, 692, L130
Ahlers, M. 2019, ApJL, 886, L18
An, Q., Asfandiyarov , R., Azzarello, P., et al. 2019, SciA, 5, eaaw3793
Antoni, T., Apel, W.D., Badea , A.F., et al. 2005, APh, 24, 1
Apel, W. D., Badea, A.F., Bekk, K., et al. 2008, APh, 29, 412
Apel, W. D., Arteaga-Velázquez, J.C., Bekk, K., et al. 2013, APh, 47, 54
Arsene, N. 2023, JCAP, 09, 020
Biermann, P. L., Becker, J.K., Dreyer, J., et al. 2010, ApJ, 725, 184
Boos, E., Lebedev, I., & Philippova, L. 2006, JPhG, 32, 2273
Burtebayev, N., Fedosimova, A., Lebedev, I., et al. 2022, Univ, 8, 67
Demidem, C., Lemoine, M., & Casse, F. 2020, PhRvD, 102, 023003
Di Sciascio, G. 2022, ApSci, 12, 705
Dmitrieva, E., Fedosimova, A., Lebedev, I., et al. 2020, JPhG, 47, 035202
Engel, R., Heck, D., & Pierog, T. 2011, ARNPS, 61, 467
Fasso, A., Ferrari , A., Sala, P. R., & Ranft , J. 2001, amcr, 955
Fedosimova, A., Kharchevnikov, P., Lebedev, I., & Temiraliev, A. 2017, EPJWC, 145, 10004
Fedosimova, A. I., Gaitinov, A. Sh., Lebedev, I. A., & Temiraliev, A. T. 2016, JPhCS, 668, 012067
Fedosimova, A. I., Olimov, Kh. K., Lebedev, I. A., et al. 2024, Parti, 7, 918
Giacinti, G., Kachelrieß, M., & Semikoz, D.V. 2018, JCAP, 7, 051
Haungs, A., Kang, D., Schoo, S., et al. 2018, EPJC, 78, 741
Heck, D., Knapp, J., Capdevielle, J. N., Schatz, G., & Thouw, T. 1998, FZKA Report 6019 (Forschungszentrum Karlsruhe)
Horandel, J. R. 2007, MPLA, 22, 1533
Ibraimova, S. A., Fedosimova, A. I., Lebedev, I. A., & Bondar, E. A. 2025, PAN, 88, 914
Kobayakawa, K., Honda, Y. S., & Samura, T. 2002, PhRvD, 66, 083004
Kvochkina, T. N., Lebedev, I. A., & Lebedeva, A. A. 2000, JPhG, 26, 35
Lebedev, I., Fedosimova, A., Mayorov, A., et al. 2021, ApSci, 11, 11189
Lebedev, I., & Boos, E. G. 2003, ICRC, 28, 259
Lipari, P. 2016, NPPP, 279, 111
Olimov, K. K., Lebedev, I. A., Fedosimova, A. I., et al. 2023, EPJP, 138, 414
Ostapchenko, S. 2011, PhRvD, 83, 014018
Ptuskin, V., Zirakashvili, V., & Seo, E. S. 2013, ApJ, 763, 47
Swordy, S. P., Fortson, L.F., Hinton, J., et al. 2002, APh, 18, 129
Tatischeff, V., Raymond, J. C., Duprat, J., Gabici, S., & Recchia, S. 2021, MNRAS, 508, 1321
Thoudam, S., & Horandel, J. R. 2012, MNRAS, 421, 1209
Tinyakov, P. G., & Tkachev, I. I. 2002, APh, 18, 165
Tomassetti, N. 2012, ApJ, 752, L13
Vladimirov, A. E., Jóhannesson, G., Moskalenko, I. V., & Porter, T. A. 2012, ApJ, 752, 68
Yuan, Q., Zhang, B., & Bi, X. J. 2011, PhRvD, 84, 043002